Performance study of electrohydrodynamic thruster under the influence of external magnetic fields

L Yethinder Ragav [1], Kadripathi KN [2], Raghu NG [3], Shusheel KC [4], Manu Jain N [5], Dr. S. Charulatha [6], Dr. Raju Garudachar [7]
Department of Aerospace Engineering
Jain University
Bengaluru, India
[1] yethinder@gmail.com, [2] kadripathi.knk@gmail.com, [3] raghunagu016@gmail.com, [4]kcshusheel@gmail.com,
[5]manujainabd2359917@gmail.com, [6] charulatha_1505@yahoo.com, [7] raju_garuda@yahoo.co.in

***Abstract*—Variation of the thrust of an electrohydrodynamic thruster by introducing an external magnetic field with different combinations of magnet positions and collector shapes is analysed. Electrohydrodynamic thruster parameters at interelectrode gap of 34 mm and pressure of 1 atm with a positive corona discharge and their interaction with external magnetic fields were investigated. The experimental setup includes an EHD thruster, a controlled chamber, a high voltage power source (HVDC), and a deflection meter to measure the thrust force. At a pressure of 1 atm, the thrust without any external magnetic field influence was 4.82 mN in the rhombus-shaped grid collector and 1.8mN in the hollow cylindrical collector, respectively. The thruster's effective thrust ranges from 1.8 mN to 5.6 mN at atmospheric pressure with an interelectrode gap of 34 mm. The introduced external magnetic field for the EHD thruster has a noticeable thrust variation in both types of collectors. However, a significant reduction in thrust-to-weight ratio across all configurations is observed because of the addition of magnets.**

Keywords— Electrohydrodynamic (EHD) thruster, magnetic field, atmospheric conditions, positive corona discharge, high voltage direct current (HVDC) power source, rhombus-shaped grid collector, hollow cylindrical collector.

I. INTRODUCTION

Undoubtedly, space research has become a hotcake for curious minds and unclassical investors. Outer space exploration is an integral part of human existence, and it is a necessary measure to widen our view and knowledge. We look deeper into space and find more potential habitats where life is possible or where we will probably live in the future other than the earth.

However, near-space observatories and satellites have equal importance in monitoring geological phenomena for human welfare. Near-space is an area extending from 20 km above the earth's surface to the Karman line. This area can be used for remote sensing, geological exploration, meteorological research, telecommunication, geographical positioning, weather forecasting, and so on. There is a need to deliver the scientific payload to near space in a cost-effective way and ensure long-term operation by compensating for orbital decay, which is not done in nanosatellites. Our ethical responsibility is to keep our space environment junk-free by removing non-operational junk satellites in orbit. Numerous studies design near-space mission-friendly thrusters to realize the need, as mentioned earlier in the space industry. However, at this height in a near-vacuum condition, airbreathing jet engines lose efficiency. The pressure is too high for ion engines, and other conventional thrusters that are presently in use, such as microjet thrusters loaded with propellants and oxidizers, are inefficient because of their low thrust-to-weight ratio [1].

It is also possible to use laser or plasma ablation thrusters for high-altitude platforms near-space applications. T. Moeller and Y. Chang simulated the laser ablation process. As a result of modelling, a laser pulse with the energy of 2 mJ provided a thrust force of 2.4 x 10^{-6} g and with a specific impulse of 80 s [2].

Another possible solution for near-space thrust generation is an electrohydrodynamic (EHD) thruster, electrically powered by a high voltage source. Such devices can have various applications: to produce the thrust, to implement near-space station-keeping manoeuvres, and to reposition [3].

Electrohydrodynamic flow study and their application are an actively developing area of research. Aircraft models based on the same have been designed with different names - electroaerodynamic (EAD) vehicles, lifters, ionocrafts [4,5,6]. The main advantages of EHD principle-based aircraft are the absence of moving parts (no propellers and high-lift devices are required), direct conversion of electrical energy into thrust, almost noiseless, high efficiency of up to 100 mN/W in the earth's atmosphere (at near-normal conditions), and a simple design [7,8].

II. ELECTROHYDRODYNAMIC PROPULSION

The motion of the electrically charged fluids is referred to as electrohydrodynamics, also known as electro-fluid-dynamics. It is the study of ionized particles or the motion of molecules and their interactions with electric fields and the surrounding fluid.

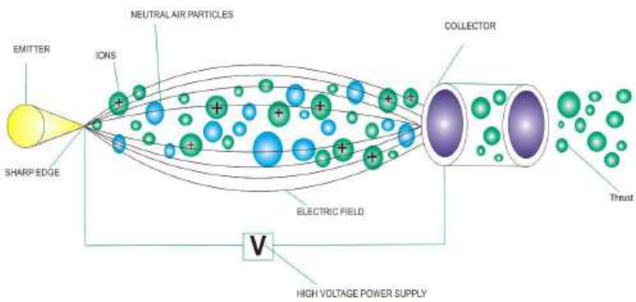

Fig. 1. Electro hydrodynamics phenomenon

It is known that atoms make up the material, and each atom has the same number of protons and electrons. When proton balances with electrons, atoms are neutral. Consider

978-1-6654-2849-1/21/$31.00 ©2021 IEEE

connecting sharp objects to the positive terminal of the high voltage power supply and smooth objects to the power supply's negative terminal. The polarities can be changed, but the emitter should always be sharp irrespective of the polarity. When the sharp object is connected to the positive terminal, the electrons from the atoms near the emitter are pulled away, leaving the atom with more positive protons than negative electrons, so these atoms are now positively charged [9,10,11].

Similarly, smooth or blunt electrodes are connected to the terminal's negative side, and the extra electron, which was stripped from the atom near the emitter, is sent to the smooth object. Hence those atoms near the emitter become positively charged. Using a sharp object at the positive terminal results in more closely packed atoms in the sharp object than the smooth object. The electric field is formed between the positive and negative terminals, as shown in figure 1. However, the electric field is more concentrated on the sharp edge of the sharp object because of the closed packing of atoms [12].

At the sharp emitter side, the electric field strength exceeds the air breakdown voltage; beyond that, surrounding electrons acquire enough energy to ionize air molecules. This electric breakdown of air is called corona discharge [12]. The electric field enormously accelerates the created ions in the region between the emitter and the collector.

While the ions are drifting towards the collecting region, they collide with neutral air molecules. The momentum transfers from charged particles to neutral particles, and this momentum transfer during the collision is responsible for the neutral wind referred to as EHD thrust [13].

III. Experimental setup

The experiment consists of 6 parts: DC Power Supply, ZVS driver, flyback transformer, deflection meter, EHD thruster, and a test chamber.

The DC Power supply produces 24 volts direct current, with a maximum capacity of 1000 Watts. It is connected to a Zero Voltage Switching (ZVS) Driver, which converts the input voltage to a high-frequency output voltage which is then stepped up to a high voltage direct current (33000V) output using a step-up transformer (flyback transfer). The EHD thruster is placed inside a test chamber which acts as a controlled environment, as shown in figure 2. The transformer's positive high voltage terminal is connected to the thruster’s emitter using a high voltage wire; the negative terminal is connected to the collector. The thruster is oriented in a horizontal direction. The thrust measuring apparatus consists of a deflection meter and a protractor attached to it.

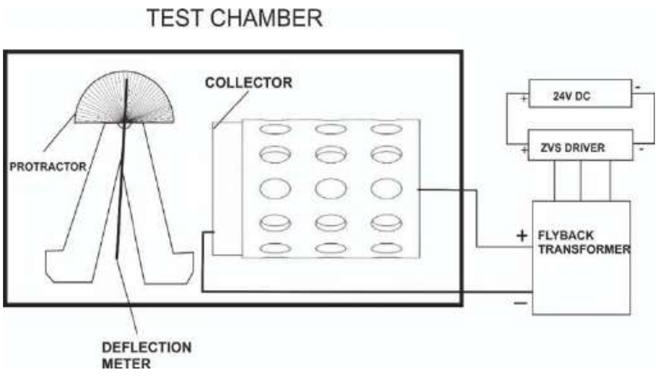

Fig. 2. Thruster in a test chamber

EHD thruster is a 3D-printed cylinder made of Polylactic Acid (PLA) plastic, as shown in figure 3. The inner diameter of the thruster is 58mm, the outer diameter is 73mm, and the length is 70mm. The thruster has 36 slots on the outer circumference, 12 in each row, to incorporate neodymium magnets. The neodymium magnet's diameter is 10mm, the thickness is 5mm, and its weight is 2.89 grams. The thruster has seven inlet holes, of which six are of 5mm diameter around a central hole of 25mm diameter. The emitter, a copper wire of 17 gauge, is wound to form a spiral shape from a total wire length of 175mm. The spiral emitter's outer diameter is 32mm, and the total height of the emitter is 36mm, which is 34mm from the collector. The emitter is placed around the central hole, concentric to the central axis of the thruster. The total weight of the thruster, emitter, and connecting wire is 38.95 grams.

Fig. 3. EHD Thruster

Two types of collectors used in this setup include aluminum foil rolled into a hollow cylinder of 70mm diameter, a width of 25mm, and a rhombus-shaped grid mesh of 189 rhombi-shaped holes with a thickness of 0.5mm, a diameter of 70mm, as shown in figure 4. The hollow cylindrical collector weighs 1.5 grams, and the rhombi-shaped grid collector weighs 2 grams. Both include the weight of the connecting wires.

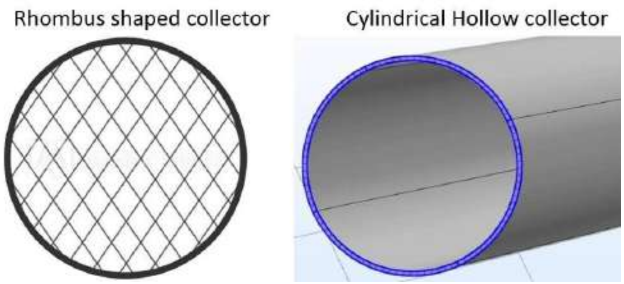

Fig. 4. Shapes of collector grid

IV. Thruster design

Various configurations, with each producing different magnetic fields, are set to study the effect of thrust force with different magnetic strengths and types of magnetic fields. Each configuration is tested with the hollow cylindrical collector and rhombus-shaped grid collector separately while maintaining all other parameters the same for all the tests with the controlled environment system's help.

A. *Configuration 1*

As shown in figure 5, no magnets are used in this contour. This setup's thrust is considered a baseline or benchmark to which other configurations' thrust is compared, as this configuration weighs the least. This system weighs 38.95 grams.

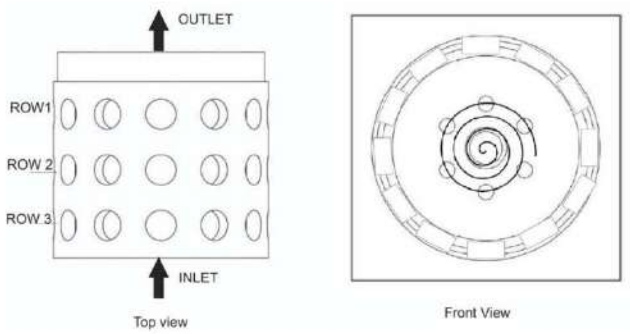

Fig. 5. Thruster design - Configuration one (C1)

B. *Configuration 2*

This setup consists of two sets of 4 magnets each, placed in their respective slots, at the top and the bottom of the thruster, as shown in row number 1 of figure 6 (top and front view). The north pole of the top 4 magnets is faced inwards, while the south pole of the bottom set of magnets faces inwards, thus creating an attractive field between the two sets. The 1st row is 20 mm from the emitter end; hence the magnetic field primarily acts only on the ionized and neutral molecules, which are being accelerated between the emitter and the collector. This setup weighs 62.07 grams, including the thruster, emitter, emitter's connecting wire, and magnets.

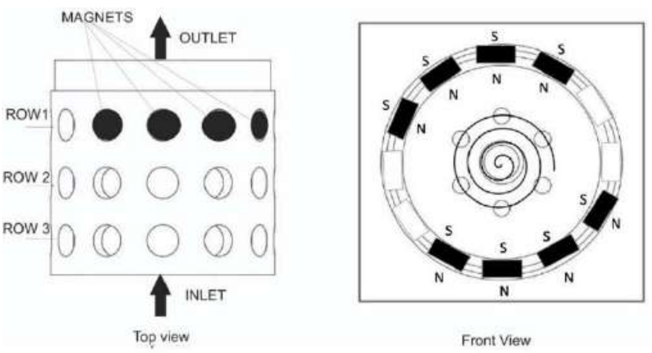

Fig. 6. Thruster design - Configuration two (C2)

C. *Configuration 3*

In this version of the setup, 24 magnets are used, with each set consisting of 12 magnets. Like in configuration two, only four slots for each set are used in row one, with each slot having three magnets stacked on top of each other, as shown in figure 7. The orientation of the magnetic poles is also similar to the second configuration. Since the number of magnets is increased, the field strength is amplified between the emitter and collector. The weight of this configuration is 108.31 grams.

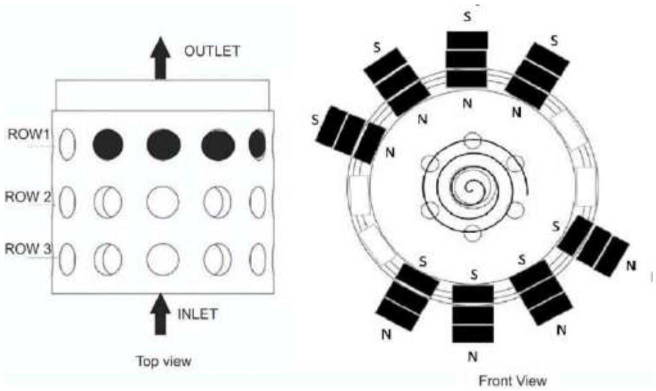

Fig. 7. Thruster design - Configuration three (C3)

D. *Configuration 4*

In this configuration, three magnets are arranged consecutively with alternating poles – North, south, and north poles facing outwards on one side; similarly, south, north, and south poles facing outwards, on the opposite side of row one, as shown in figure 8. The weight of this arrangement is 73.63 grams.

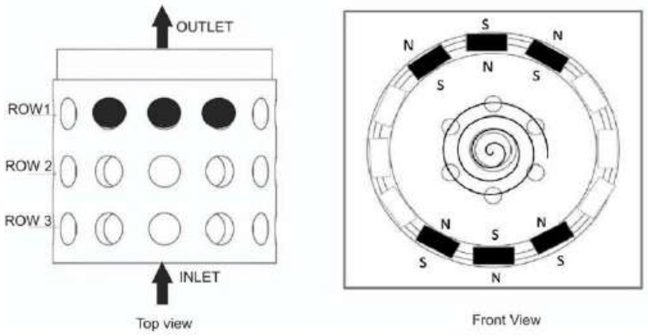

Fig. 8. Thruster design - Configuration four (C4)

E. *Configuration 5*

All 36 slots of the thruster are filled with magnets in this system, as shown in figure 9. All the magnets' north pole face toward the centre of the thruster; thus, a repulsive magnetic field is spread throughout the thruster. This setup weighs the heaviest at 142.99 grams.

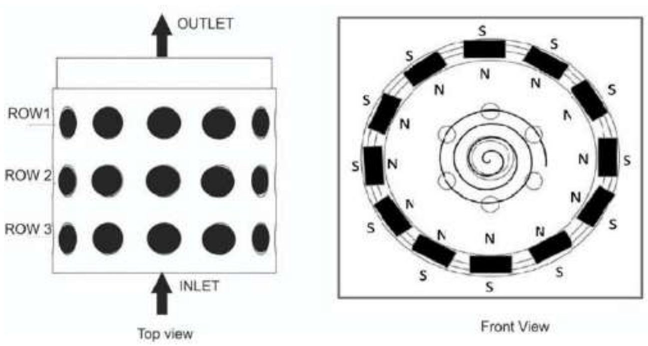

Fig. 9. Thruster design - Configuration five (C5)

V. THRUST MEASUREMENT

The requirement for precise satellite positioning and orbital manoeuvring is increasing with the advancement in space technology. This, in turn, demands a need for precise thrust measurement techniques for micro-scale thrusters. Conventional methods like load cell-based thrust measurement are not suitable for this purpose because low values of the thrust are produced, which are significantly affected by the amplifier's background noise, and small impulse from the thruster remains unnoticed [14]. Moreover, the intense magnetic field applied over the thruster to study the characteristic thrust performance seems to disturb the load cell's output. The results obtained from the milligram load cell were uncertain because of high electromagnetic interference between the cell and the applied external magnetic field. Hence a simple pendulum-based thrust measurement setup is designed, as shown in figure 10. By resolving the resultant forces acting on the pendulum to produce the deflection θ, the thrust force is calculated indirectly through mathematical modelling. This method may not be perfect for absolute thrust calculation, but it serves to compare the thrust of various setups while maintaining other parameters constant.

A. *Design specification and mathematical modelling*

A freely oscillating pendulum is fixed to rigid support at the point so that it has only two degrees of freedom. The pendulum base area is equal to the thruster exit area; hence it is assumed that all the thrust force is directly acting on the pendulum base with negligible loss of energy to the surrounding. The thruster is placed horizontally such that its collector is at a distance of 60 millimetres from the pendulum's mean position. The total mass of a freely moveable part of a pendulum is one gram; hence 9.8×10^{-3} Newtons of force is acting on it due to the earth's acceleration due to gravity (g). Thruster, which is placed horizontally facing the pendulum, tries to push it, let θ be the pendulum's deflection because of the interaction between these two perpendicular forces. Hence resolving the resultant force will give the thrust value.

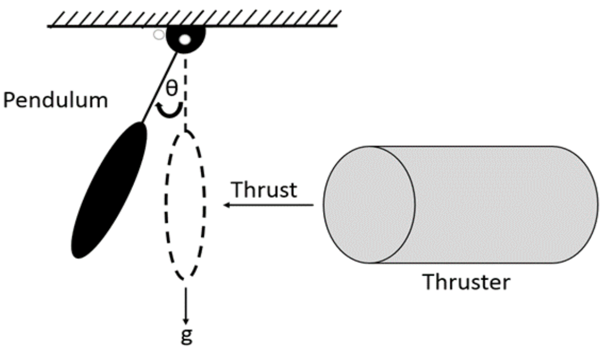

Fig. 10. Illustration of the thrust measurement setup

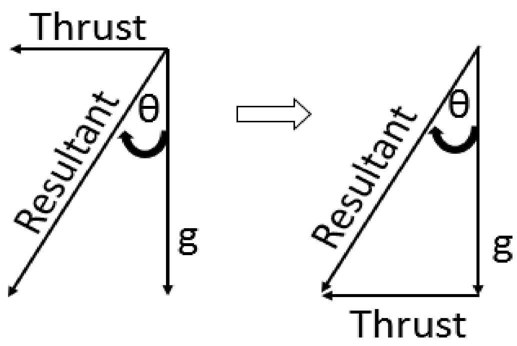

Fig. 11. Force resolution and Force triangle

From the figure 11,

$$\tan\theta = \text{Thrust}/g \tag{1}$$

Therefore,

$$\text{Thrust} = g \times \tan\theta \tag{2}$$

Where $g = 9.8 \times 10^{-3}$ Newtons and θ in degrees.

The accuracy and sensitivity of a thrust bench depend on the sensor used and the thrust measurement mode. Both direct and indirect measurements are used in the space industry, but always direct measurements are given preference because of better precision in the case of microsatellites [15]. If the micro-thruster itself is mounted on the test bench, it gives a direct measurement of the thrust force, but if the thruster's exhaust is used to produce deflection, as in the pendulum setup, it is an indirect method. Problems in indirect thrust measurements are associated with dissipation of energy as unknown elasticity during the momentum exchange between the exhaust plume particles and the target (pendulum) [16,17]. However, this method can be effectively used to approximate the change in thrust during different testing configurations while maintaining all other parameters constant. The loss of energy in indirect measurement is the same for the constant distance between thruster and the pendulum's mean distance [18,19,20].

VI. RESULTS

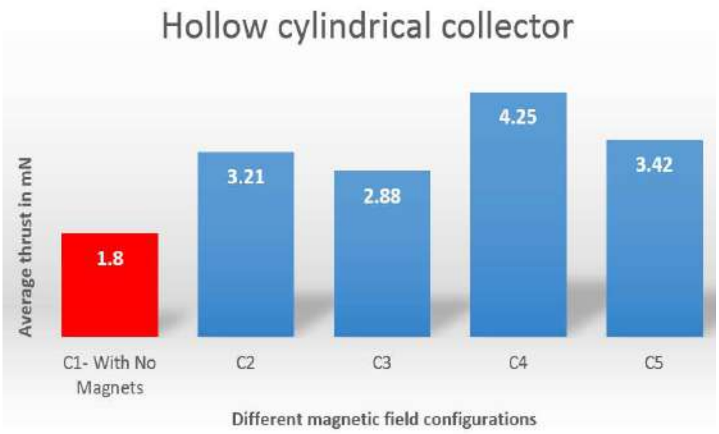

Fig. 12. Graph of thrust force with hollow cylindrical collector with different configurations of magnetic field

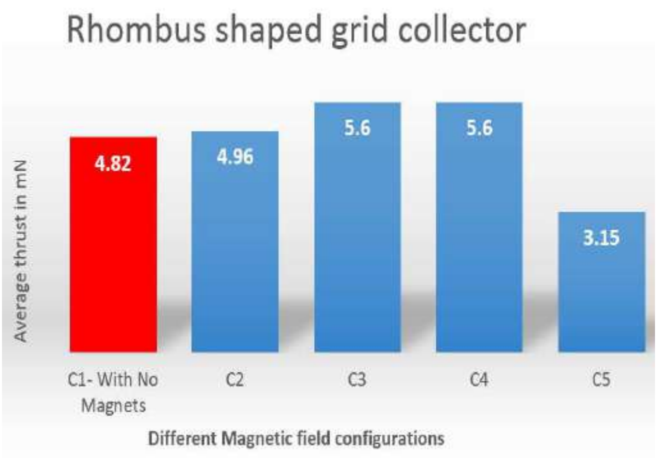

Fig. 13. Graph of thrust force with rhombus-shaped grid collector with different configurations of magnetic field

The tests are performed in a controlled environment, five times each for each collector-configuration combination, and the average thrust is considered for the final result.

For the hollow cylindrical collector, as shown in figure 12, the highest thrust, 4.25 mN, is produced by configuration 4. The basic setup, with no magnets, configuration 1, produced a thrust of 1.8 mN, which is also the least. Configurations 2 and 5 produced almost the same thrust of 3.21 mN and 3.42 mN, respectively. Configuration 3 gave out an average thrust of 2.88 mN, which is the second-lowest. Overall, the variation of thrust is considerable, with a maximum difference of almost 2.45 mN.

With the rhombus-shaped grid collector, thrust variation is not significant in most cases. As shown in figure 13, the lowest thrust, 3.15 mN, was observed with the 5th configuration. 5.6 mN, which is the highest thrust, was seen in both the 3rd and 4th configurations. The 1st and 2nd configurations produced 4.82 mN and 4.96 mN, respectively.

VII. Conclusion

The results depict that the thrust of an EHD thruster can be effectively increased by applying a magnetic field around it. Different configurations of magnetic fields and their effects are discussed in the results section.

Among various configurations of collector shapes and magnetic fields – a rhombus-shaped grid in configurations 3 and 4 performed better than others.

Rhombus or honeycomb-like structured collector shapes are efficient because they can provide maximum electric field exposure and maximum contact area along the path of the ions and energize them. In contrast, a hollow collector produces a low value of average thrust because the collector's electric field is just confined to the edge walls, and its design constitutes less collector area on average. Hence, a hollow cylindrical collector whose regions are just confined to the edge walls cannot optimize the thrust.

In the rhombus grid with configuration 5, where only the north pole faces the center, there is a significant decrease in thrust. The accelerated ions produce a magnetic field around them, which has both the north pole and south pole, but the applied magnetic field's north pole is dominant. This opposes the ion's magnetic field growth; due to the opposition, ions decelerate and lose kinetic energy. Hence same pole magnet facing the center will decrease the thrust. However, this configuration is slightly effective with the hollow cylindrical collector compared to configurations 2 and 3. This is possible because of the combined field of all the magnets, which is strong only near the wall, therefore attracting and keeping the ions near the wall, which is beneficial as the electric field of the hollow cylindrical collector acts mainly at the wall. Due to the more than usual density of the ions near the wall, the hollow cylindrical collector can accelerate more ions, thus, producing a higher thrust. In contrast, the rhombus grid produces a lower thrust as the collector area near the wall is smaller.

Magnetic fields of configurations 2 and 3 reconstruct mostly across the circular cross-section and perpendicular to charged particle motion. In these circumstances, Lorentz force acts towards the thruster's wall, and the frequency of particle collision with the wall increases slightly. As a consequence, they lose their kinetic energy, and the thrust drops a little. While most of the field lines are perpendicular to the cross-section, some part of the field also acts along the circumference. In figure 6 and figure 7, the magnets at either end will have a field between themselves and the opposite pole magnets on the other side, along the circumference. This field is stronger in configuration 3. In configuration 4, most of the magnetic field reconstructs along the inner circumference of the thruster. When the fields are along the circumference, they act as a boundary layer. It reduces the collision of charged particles with the thruster wall; hence particles travel with maximum energy they possess in a streamlined path and contribute to the thrust. Thus magnetic fields confined to the thruster's inner boundary is advantageous, which is evident in both types of collectors.

The stronger the field is along the inner circumference, the lower the losses due to wall collisions. This is apparent in the results of the rhombus collector (C2 and C3); however, the opposite is true with the hollow cylindrical collector. It is because the stronger field will divert the charged particles away from the wall, and since the electric field strength of the hollow collector diminishes towards the center, the thrust produced is lower than that of configuration 2.

Table I. Thrust to weight ratio

	Collector Shape- Thrust to weight ratio	
Configurations	Rhombus shaped collector	Hollow cylindrical collector
Configuration 1	0.0120	0.00248
Configuration 2	0.0078	0.00235
Configuration 3	0.0052	0.00177
Configuration 4	0.0076	0.00373
Configuration 5	0.0022	0.00150

On adding magnets to the thruster, there is a notable increase in the thruster's weight, which causes a decrease in the thruster's thrust-to-weight ratio, as shown in Table 1. So, if magnets are needed to be added at all, it is recommended to add magnets in configuration 4, as the thrust-to-weight ratio is maximum compared to any other configuration with magnets. However, the thruster with no magnets tops the thrust-to-weight ratio, and hence it is suggested not to use magnets for the best performance output. Moreover, the thruster does not have to be as heavy as it is in this setup for the same thrust output; it can be much lighter with lightweight materials or just by using the emitter and the collector (without the body).

ACKNOWLEDGMENT

We would like to express our deep gratitude to Professor Raju Garudachar and Professor S Charutatha, our project guides, for their patient guidance, enthusiastic encouragement, and useful critiques of this research work that greatly improved the manuscript.

We would also like to show our gratitude to Dr. Ramesh Gopalan, Dean & HoD, Gopalan College of Engineering and Management, for sharing their pearls of wisdom with us during the course of this research and motivated the team to carry out the research.

REFERENCES

[1] I.V. Mostoslavsky, Aircraft aerodynamics (Russian edition aerodynamics sample), Book on Demand Ltd., Moscow, 2019.

[2] T. Moeller, Y.-K. Chan, MACH 2 Simulations of a micro laser ablation plasma thruster, Aerospace Science and Technology (2007) 481–489.

[3] E. van Wynsberghe, A. Turak, Station-keeping of a high-altitude balloon with electric propulsion and wireless power transmission: A concept study, Act Astronautica. 128 (2016) 616–627.

[4] K. Masuyama, Performance characterization of electrohydrodynamic propulsion devices, Massachusetts Institute of Technology, 2012.

[5] K. Masuyama, S.R.H. Barrett, On the performance of electrohydrodynamic propulsion, Proc. Math. Phys. Eng. Sci. 469 (2154) (2013), 20120623–20120623.

[6] N.A. Gatsonis, Y. Lu, J.J. Blandino, M.A. Demetriou, N. Paschalidis, Micropulsed plasma thrusters for attitude control of a low-earth-orbiting cubesat, 54th AIAA Aerospace Sciences Meeting, 2016, 0692.

[7] B. Goksel, ¨ I.C. Mashek, First breakthrough for future air-breathing magneto-plasma propulsion systems, Journal of Physics.: Conf. Ser. 825 (1) (2017), 012005.

[8] D.S. Drew, K.S.J. Pister, First takeoff of a flying microrobot with no moving parts, in: 2017 International Conference on Manipulation, Automation and Robotics at Small Scales (MARSS), 2017, pp. 1–5.

[9] C.K. Gilmore, S.R.H. Barrett, Electrohydrodynamic thrust density using positive corona-induced ionic winds for in-atmosphere propulsion, Proc. Math. Phys. Eng. Sci. 471 (2175) (2015), 20140912–20140912.

[10] L. Pekker, M. Young, Model of ideal electrohydrodynamic thruster, Journal of Propulsion. Power 27 (4) (2011) 786–792.

[11] E. Moreau, N. Benard, J.-D. Lan-Sun-Luk, J.-P. Chabriat, Electrohydrodynamic force produced by a wire-to-cylinder dc corona discharge in air at atmospheric pressure, Journal of Applied Physics. 46 (47) (2013) 475204.

[12] L. Pekker, M. Young (2010). A model of an ideal electrohydrodynamic thruster. From researchgate.net

[13] Nicolas Monrolin, Franck Plouraboué, Olivier Praud (2017). Electrohydrodynamic thrust for in-atmosphere propulsion. From hal.archives-ouvertes.fr

[14] Mueller, J., Hofer, R., & Ziemer, J. (2010). Survey of propulsion technologies applicable to cubesats. Retrieved August 11, 2017, from https://ntrs.nasa.gov/search.jsp?R=20100032899.

[15] Bijster, R. J. F. (2014). Design, verification and validation of a micropropulsion thrust stand (Doctoral dissertation), Delft University of Technology, Delft, Netherlands.

[16] Jean-Yves (2006). Test bench for pop-pop engines. [Web log post]. Retrieved August 11, 2017, from http://www.eclecticspace.net/poppop/jy/Test_bench_for_pop-pop_engines_V3.1.pdf

[17] Marhold K, Tajmar M. Direct thrust measurement of in-FEEP clusters. IEPC2005-235. Princeton University; 2005.

[18] Phipps CR, Luke JR, Helgeson WD. A 25 nN low-noise thrust stand for microthrusters. IEPC-2005-318. Princeton University; 2005.

[19] S. Chakraborty, "An electrostatic ion-guide and a high-resolution thruststand for characterization of micro-propulsion devices," Ph.D. dissertation (EPFL, Switzerland, 2015).

[20] S. Chakraborty, C. Ataman, S. Dandavino, and H. Shea, in Proceedings of PowerMEMS, Atlanta, USA, 2-5 December 2012, pp. 528–53